Clusterin in Alzheimer's disease: an amyloidogenic inhibitor of amyloid formation

Panagiotis M. Spatharas[1], Georgia I. Nasi[1], Paraskevi L. Tsiolaki[1, †], Marilena K. Theodoropoulou[1], Nikos C. Papandreou[1], Andreas Hoenger[2], Ioannis P. Trougakos[1], Vassiliki A. Iconomidou[1, *]

[1] Section of Cell Biology and Biophysics, Department of Biology, School of Sciences, National and Kapodistrian University of Athens, Panepistimiopolis, Athens 157 01, Greece

[2] University of Colorado at Boulder, Department of Molecular, Cellular and Developmental Biology, Boulder, CO 80309-0347, USA

[†] Present Address: Department of Biochemistry and Biophysics, University of California, San Francisco, California 94143-2240, USA

[*] Corresponding author: veconom@biol.uoa.gr

e-mails:

Panagiotis M. Spatharas: panspatharas@biol.uoa.gr

Georgia I. Nasi: gnasi@biol.uoa.gr

Paraskevi L. Tsiolaki: etsiolaki@biol.uoa.gr

Marilena K. Theodoropoulou: mtheod@biol.uoa.gr

Nikos C. Papandreou: npapand@biol.uoa.gr

Andreas Hoenger: Andreas.Hoenger@Colorado.edu

Ioannis P. Trougakos: itrougakos@biol.uoa.gr

Vassiliki A. Iconomidou: veconom@biol.uoa.gr

Word count: Abstract – 129 words, Introduction – 747 words, Results – 1764 words, Discussion – 1853 words, Materials and Methods – 1447 words, Figure and Table legends – 927 words

Keywords: Clusterin, Molecular chaperones, Aggregation-prone regions, Amyloid, Amyloid-*β*, Amyloid inhibitors, Alzheimer's disease

Abstract

Clusterin is a heterodimeric glycoprotein (α- and β-chain), which has been described as an extracellular molecular chaperone. In humans, clusterin is an amyloid associated protein, co-localizing with fibrillar deposits in several amyloidoses, including Alzheimer's disease. To clarify its potential implication in amyloid formation, we located aggregation-prone regions within the sequence of clusterin α-chain, via computational methods. We had peptide-analogues of each region chemically synthesized and experimentally demonstrated that all of them can form amyloid-like fibrils. We also provide evidence that the same peptide-analogues can inhibit amyloid-β fibril formation. These findings elucidate parts of the molecular mechanism in which clusterin inhibits amyloid formation. At the same time, they hint that molecular chaperones with amyloidogenic properties might have a role in the regulation of amyloid formation, essentially acting as functional amyloids.

38 **Introduction**

39 Since the 17th century, physicians had already started to describe clinical disorders that were
40 later included in a broad group of diseases, nowadays known as amyloidoses (Kyle, 2011). Prime
41 examples are Alzheimer's disease (AD), Parkinson's disease, type 2 diabetes and AL amyloidosis
42 (Benson *et al*, 2020). It is widely considered that these diseases are closely associated with the
43 accumulation and close packing of normally soluble proteins, which end up creating highly
44 ordered, insoluble aggregates. The so called amyloid fibrils, are deposited extracellularly in
45 organs or tissues, causing significant damage (Benson *et al.*, 2020).

46 Molecular chaperones can inhibit amyloid formation in its early stages, thus preventing amyloid-
47 related cytotoxicity (Wentink *et al*, 2019). Recent studies though, have shown that molecular
48 chaperones can have amyloidogenic properties (Ecroyd & Carver, 2009; Ecroyd *et al*, 2010;
49 Niewold *et al*, 1999; Tsiolaki *et al*, 2017), despite their seemingly contradicting physiological
50 function. *In vitro* experiments performed by our team have hinted that clusterin could be such a
51 protein (Tsiolaki *et al.*, 2017). Clusterin is a ubiquitous, conserved mammalian glycoprotein,
52 whose main isoform is secreted and has been described as an extracellular molecular chaperone
53 (Jones & Jomary, 2002). Human clusterin precursor is a 449 residue-long polypeptide chain,
54 which, after having its signal peptide removed, is reduced to 427 residues, and goes through
55 several post-translational modifications (Jones & Jomary, 2002). Mature clusterin is cleaved in
56 two chains —α-chain, consisting of 222 residues and β-chain, consisting of 205 residues— with
57 five disulfide bonds forming between them (Jones & Jomary, 2002). Its molecular weight is
58 approximately 80 kDa, almost 30% of it being carbohydrates, added by glycosylation (Jones &
59 Jomary, 2002). Clusterin's structure has yet to be experimentally determined, but is believed to
60 contain three long molten globule-like regions and five amphipathic α-helices, which allow for
61 hydrophobic interactions with its client-proteins (Bailey *et al*, 2001).

62 Under normal circumstances, clusterin exists in solution as heterogeneous aggregates (Poon *et*
63 *al*, 2002). It has been suggested that, at mildly acidic pH (Poon *et al.*, 2002), these aggregates
64 disassociate and the disassociated chaperone-active subunits function in an ATP-independent
65 manner (Poon *et al*, 2000). They bind misfolded client-proteins and form a high molecular
66 weight complex. The formation of the complex allows for stabilization of the misfolded
67 proteins, which are consequently refolded by other molecular chaperones (Bailey *et al.*, 2001)
68 (visualized in Fig 1). Clusterin's ever-growing list of known clients includes a variety of proteins,
69 such as cellular receptors, apolipoproteins, the complement complex, immunoglobulins,
70 amyloid-forming proteins and non-protein molecules, like lipids and heparin (Calero *et al*, 2005).

71 Having such a broad range of clients, it is only logical that clusterin contributes in many
72 physiological and pathological processes (Rohne *et al*, 2016). AD is one of the most notable
73 pathologies in which clusterin is involved (Calero *et al.*, 2005). Consistent with its chaperone
74 function, clusterin keeps the amyloid-*β* (A*β*) peptide soluble while transporting it in biological
75 fluids, modulates its permeation through the blood-brain barrier and contributes to its
76 clearance, effectively halting amyloid formation (Matsubara *et al*, 1996). In direct contradiction
77 to that, it has been reported that clusterin contributes to the early stages of AD pathogenesis
78 (DeMattos *et al*, 2002; Oh *et al*, 2019). To this day, clusterin's role in AD is yet to be fully
79 understood. Despite the mystery surrounding clusterin's implication in AD, it is a known fact
80 that it co-localizes with A*β* fibrillar deposits (Calero *et al.*, 2005). This is also true for other
81 amyloidoses, in which clusterin is an amyloid associated protein (Nastou *et al*, 2019).

82 It can be assumed that clusterin is found in the amyloid deposits because it is drifted along by its
83 client-proteins. In this study, we examined a different scenario, one that doesn't rule out the
84 possibility of clusterin being amyloidogenic itself. We used AMYLPRED (Frousios *et al*, 2009), a
85 consensus algorithm for the prediction of amyloid propensity, in order to identify aggregation-
86 prone regions in clusterin *α*-chain. We had peptide-analogues of each region chemically
87 synthesized and experimentally demonstrated that all of them can form amyloid-like fibrils *in*

88 *vitro*. The same peptide-analogues, despite being amyloidogenic, can inhibit A*β* fibril formation.
89 Based on our findings, we proposed a putative mechanism in which clusterin prevents amyloid
90 formation. The suggested mechanism could also explain the contradictory reports that hint at
91 clusterin's implication in the acceleration of the appearance of AD symptoms. At the same time,
92 we hope that the basis of clusterin's amyloid inhibiting activity could give insight into the
93 implementation of peptide-based amyloidogenesis inhibitors in the treatment of amyloidoses.

94 Results

95 All wild-type clusterin *α*-chain peptide-analogues form amyloid-like fibrils *in vitro*

96 According to the prediction of AMYLPRED, clusterin *α*-chain has five aggregation-prone regions.
97 The peptide-analogues that correspond to those regions are NFHAMFQ, AMDIHF, ILSVD,
98 YYLRVTT and EVVVKLF, as depicted in Fig 2. NFHAMFQ has previously been studied by our lab
99 and proved to exhibit amyloidogenic properties *in vitro* (Tsiolaki *et al.*, 2017). Our current
100 findings reveal that AMDIHF, ILSVD, YYLRVTT, and EVVVKLF can also be characterized as
101 amyloidogenic *in vitro*, making a total of five experimentally verified aggregation-prone regions
102 in clusterin *α*-chain. Characterization was based on the tinctorial criteria, which are commonly
103 used for the identification of amyloid fibrils (transmission electron microscopy, X-ray diffraction
104 from protein fibers, ATR FT-IR spectroscopy and Congo Red birefringence assay) (Sunde & Blake,
105 1998).

106 Transmission electron micrographs show that AMDIHF, ILSVD, YYLRVTT, and EVVVKLF self-
107 assemble into amyloid-like fibrils (Fig 3 A-D, respectively). AMDIHF fibrils exhibit considerable
108 polymorphism, forming both supercoils and tapes (Fig EV1 A-C), while EVVVKLF fibrils form large
109 twisting ribbons, with a 162 nm pitch (Fig EV1D). ILSVD forms amyloid-like fibrils that are
110 packed more densely in comparison to the other peptides (Fig 3), indicating that it could be the
111 most aggregation-prone region in clusterin α-chain.

112 Oriented fibers formed by each peptide solution, produce X-ray diffraction patterns, indicative
113 of the presence of the "cross-*β*" structure. Most reflections are ring-like, most likely because
114 the fibrils are not perfectly aligned in a parallel manner (Makin & Serpell, 2005). The exact
115 measurements for each of the four diffraction patterns can be seen in Fig 3 (E-H). It is worth
116 pointing out that EVVVKLF diffraction pattern has two equatorial reflections, one at 8.12 and
117 one at 12.12 Å. Upon closer examination of the twisting ribbons, formed by EVVVKLF (Fig
118 EV1D), the maximum width is observed in the middle of the pitch, and measures approximately
119 53 nm, while the minimum width is observed at the site of the twist, and measures
120 approximately 35 nm. The quotient of the two equatorial reflections (8.12 : 12.12 ≈ 0.67) is
121 roughly equal to the quotient of the minimum and maximum ribbon width (35 : 53 ≈ 0.66). The
122 equatorial reflections are indicative of the distance between packed beta sheets. Thus, EVVVKLF
123 fibrillar structures are probably formed by β-sheets that are more tightly packed at the twist, in
124 comparison to the middle of the ribbon. The periodicity of the tightening and untightening of
125 the β-sheets is revealed by a combination of X-ray and TEM data.

126 The dominance of the *β*-sheet secondary structure is supported by ATR FT-IR spectroscopy data,
127 since the spectra of all four peptide-analogues reveal bands that can be assigned to *β*-sheets
128 (Surewicz *et al*, 1993) (Table 1 and Fig 3 M-O).

129 Every peptide binds Congo Red, as seen under bright field illumination in a polarizing
130 stereomicroscope (Fig 3 I-L, upper). When the polars are crossed, the peptides exhibit the
131 apple-green birefringence (Fig 3 I-L, lower) that amyloids typically exhibit.

132 **NLSVD, a mutant counterpart of ILSVD, does not exhibit amyloidogenic properties**

133 Recent studies have identified a novel pathological mutation on clusterin's gene, in AD patients.
134 In particular, p.I360N changes the aggregation-prone region ^{81}ILSVD^{85} to ^{81}NLSVD^{85} (Bettens *et*
135 *al*, 2015). The resulting sequence is not predicted by AMYLPRED, hinting that it is not
136 aggregation-prone. To experimentally confirm that the mutated region is not aggregation-

137 prone, we had NLSVD chemically synthesized. Indeed, transmission electron microscopy (TEM)
138 shows that NLSVD does not self-assemble into amyloid fibrils (Fig EV2A). Also, NLSVD does not
139 form oriented fibers, suitable for X-ray diffraction, hinting that there are no fibrils in its solution.
140 Finally, when stained with Congo Red and stereoscopically observed between crossed polars, it
141 does not exhibit apple-green birefringence (Fig EV2B).

142 **Clusterin *α*-chain peptide-analogues inhibit A*β*$_{42}$ amyloid formation *in vitro***

143 Full-length clusterin is known to inhibit A*β* fibril formation *in vitro* (Yerbury *et al*, 2007). We
144 aimed to pinpoint segments of its sequence that could act as catalysts of said inhibition. Each
145 clusterin peptide-analogue was co-incubated with equimolar amounts of A*β*$_{42}$ and the
146 aggregation kinetics were evaluated with Thioflavin T (ThT) fluorescence measurements over
147 time and TEM.

148 ThT fluorescent measurements reveal that individual A*β*$_{42}$ starts forming fibrils almost
149 immediately and reaches maximal fluorescence signal after approximately 7 hours. When co-
150 incubated with clusterin peptide-analogues (A*β*$_{42}$+NFHAMFQ, A*β*$_{42}$+AMDIHF, A*β*$_{42}$+ILSVD,
151 A*β*$_{42}$+YYLRVTT, and A*β*$_{42}$+EVVVKLF), A*β*$_{42}$ exhibits decreased emission. ILSVD and especially
152 EVVVKLF seem to be the most potent inhibitors (Fig 4J and 4P, respectively). As previously
153 shown, individual ILSVD is incredibly amyloidogenic, as is A*β*$_{42}$. The fact that interaction
154 between the two leads to decreased fibril formation, hints that peptides with high
155 amyloidogenic potential, could negate each other's fibril-forming properties. EVVVKLF bears
156 some sequence similarity with ^{16}KLVFFA^{21}, a key amyloid-forming segments of A*β*$_{42}$ (Lu *et al*,
157 2019). Considering that peptide-analogues derived from ^{16}KLVFFA^{21} have been suggested as
158 potential therapeutic agents for the treatment of AD (Chafekar *et al*, 2007), it is not surprising
159 that EVVVKLF has the highest inhibiting effect among the five peptides. NFHAMFQ and AMDIHF
160 also seem to inhibit A*β*$_{42}$ fibril formation (Fig 4F and 4H, respectively), but their potential as
161 inhibitors is less significant than that of ILSVD and EVVVKLF. YYLRVTT effectively delays fibril
162 formation, but after approximately 20 hours, fluorescence signal begins to rise (Fig 4N). After 40

163 hours, Aβ_{42}+YYLRVTT reaches fluorescence intensity levels which are comparable to those of
164 individual Aβ_{42}.

165 TEM confirms that all five peptide-analogues inhibit or delay Aβ_{42} fibril formation, after 7 days of
166 incubation. When individually incubated, Aβ_{42} forms straight and unbranched fibrils with
167 indefinite length and a diameter of approximately 80 Å (Fig 4 B-D). A small number of fibrils is
168 observed after 1 day of incubation (Fig 4B). The population of fibrils increases significantly after
169 3 days (Fig 4C) and reaches its maximum after 7 days (Fig 4D). As expected, ILSVD and EVVVKLF
170 prove to be the most potent inhibitors (Fig 4I and 4O, respectively). The entire grids were
171 thoroughly examined, and no fibrils were observed. NFHAMFQ and AMDIHF also inhibit Aβ_{42}
172 fibril formation, as fibrils were not observed anywhere on the grid (Fig 4E and 4G, respectively).
173 However, both seem to induce the formation of amorphous aggregates. YYLRVTT seems to
174 delay, but not inhibit fibril formation. In contrast to the other peptides, fibrils can be observed
175 (Fig 4M). The number of fibrils is similar to that of individual A$\beta_{42,}$ after 1 day of incubation.
176 Much like NFHAMFQ and AMDIHF, YYLRVTT also seems to induce the formation of amorphous
177 aggregates.

178 On the contrary, ThT kinetics and TEM show that NLSVD, the mutant counterpart of ILSVD, does
179 not inhibit Aβ_{42} amyloid formation *in vitro*. Aβ_{42} and Aβ_{42}+NLSVD fluorescence curves mostly
180 overlap, while Aβ_{42}+NLSVD show a slightly enhanced fluorescence peak (Fig 4K). Transmission
181 electron micrographs reveal that Aβ_{42} fibril morphology is different to that of Aβ_{42}+NLSVD.
182 Aβ_{42}+NLSVD fibrils, after 7 days of incubation, are more densely packed and slightly wider than
183 those of individual Aβ_{42}, after the same incubation period (Fig 4L and Fig EV2C, white arrow).
184 Furthermore, Aβ_{42}+NLSVD fibrils tend to interact laterally and form loosely bound tapes (Fig
185 EV2C, blue arrows).

186 **Computational insight into the inhibition of Aβ_{42} fibril formation by EVVVKLF**

187 To shed light on the interaction between Aβ_{42} and EVVVKLF, the most potent of the five peptide-
188 inhibitors, molecular dynamics simulations were performed, using an NMR structure of
189 pentameric Aβ_{42} (PDB ID: 2BEG) (Luhrs *et al*, 2005). A structure for EVVVKLF was generated
190 through the "Builder" tool in PyMOL (Delano, 2005). Molecular docking was performed through
191 the automated protein docking server ClusPro (Kozakov *et al*, 2013; Kozakov *et al*, 2017; Porter
192 *et al*, 2017; Vajda *et al*, 2017). The generated clusters were evaluated with the balanced scoring
193 scheme. Following energy minimization, the interaction between Aβ_{42} key amyloid-forming
194 segment ^{17}LVFFA^{21} (Fig 5A, dark grey) and EVVVKLF (Fig 5A, light grey) was ascertained (Fig 5A,
195 left). Aβ_{42}+EVVVKLF complex structural stability was monitored through per-residue root mean
196 square fluctuation (RMSF) calculation, as well as time-dependent root mean square deviation
197 (RMSD) measurements (Fig 5B and 5C, respectively). After 600 ns of molecular dynamics
198 simulations, a complex dissociation has occurred, significantly changing the conformation of the
199 pentamer, in comparison to its original state (Fig 5A). The C-termini of all five chains are
200 characterized by large fluctuations (0.4 – 0.8 nm), with chains-A and -B exhibiting the highest
201 mobility. In contrast, the N-termini of the aforementioned chains exhibit the lowest mobility
202 among all chains, while chain-E N-terminus is characterized by fluctuations of over 0.8 nm.
203 Secondary structure analysis was performed using the dictionary of secondary structure of
204 proteins (DSSP) algorithm (Kabsch & Sander, 1983; Touw *et al*, 2015) and reveals that β-sheet
205 content gradually decreases (Fig 5D). Intermolecular hydrogen bonds are formed, even before
206 the simulation has begun, and reach a maximum number of 12 (Fig 5E). Upon examination of
207 the last frame of the simulation (Fig 5A, right), EVVVKLF has partly adopted a β-strand
208 conformation. Using UCSF Chimera and the "FindHBond" tool (Pettersen *et al*, 2004), we show
209 that EVVVKLF forms three possible hydrogen bonds with the chain-A ^{16}LVFFA^{21} region, becoming
210 a part of an intermolecular β-sheet. EVVVKLF also forms hydrogen bonds with the C-terminus of
211 the A-chain. By forming hydrogen bonds with both regions, it essentially stiches the N-terminal
212 ^{17}LVFFA^{21} to the C-terminus. The fact that RMSF values are low for the N-terminus and high for

213 the C-terminus hints that the later moves towards the former. In this way, fibril elongation from
214 chain-A could be blocked. The addition of more than one peptide-inhibitors could promote
215 interactions with chain-E, effectively blocking both elongation epitopes of the pentamer.

216 **Natively disordered regions in human clusterin α-chain**

217 Human clusterin is believed to have three long molten globule-like regions (Bailey *et al.*, 2001).
218 PONDR® VLTX (http://www.pondr.com) predicts five natively disordered regions in clusterin α-
219 chain (Fig 6), the longest of which is located at the C-terminus. All five aggregation prone
220 regions are located near predicted natively disordered regions. ^{12}NFHAMFQ^{18} is on the right of
221 the N-terminal natively disordered region and on a putative amphipathic *α*-helix (Bailey *et al.*,
222 2001). Putative *α*-helices are believed to be implicated in the interaction between clusterin and
223 its client proteins (Bailey *et al.*, 2001). ^{30}AMDIHF^{35} is located directly to the right of said putative
224 amphipathic *α*-helix. ^{81}ILSVD^{85} is surrounded by two natively disordered regions. ^{155}YYLRVTT^{161}
225 is also located directly to the left of a natively disordered region, while ^{177}EVVVKLF^{183} is partly
226 predicted as natively disordered. Interestingly, the EVVVKLF peptide-analogue adopts *β*-sheet
227 secondary structure, according to the ATR FT-IR spectrum (Fig 3P). The proximity of all five
228 aggregation-prone regions to natively disordered regions may hint that, due to the flexibility of
229 the later, the former could act semi-independently of the protein.

230 ## Discussion

231 **Full-length clusterin could also have amyloidogenic properties *in vitro***

232 Recent studies have shown that short aggregation-prone segments, known as amyloidogenic
233 determinants, can lead to amyloid formation, even when they are inserted in non-
234 amyloidogenic proteins, via protein engineering (Teng & Eisenberg, 2009). The fact that
235 clusterin has five such segments in its *α*-chain, provides potent indication that the *α*-chain and

236 consequently the full-length protein, may intrinsically exhibit amyloidogenicity. This argument
237 has fascinating implications, especially considering clusterin's role as a molecular chaperone.

238 **Molecular chaperones and their involvement in amyloid formation and inhibition**

239 One of the fundamental functions of molecular chaperones is considered to be the prevention
240 of protein aggregation and consequently, amyloid fibril formation (Wentink *et al.*, 2019). Based
241 on that notion, it has been suggested that molecular chaperones could be used as anti-amyloid
242 drugs (Yerbury & Kumita, 2010). In direct contradiction to that, clusterin has the potential to
243 form amyloid-like fibrils. In fact, there have been reports of other proteins that function as
244 molecular chaperones and exhibit amyloidogenicity *in vitro* (Ecroyd & Carver, 2009; Ecroyd *et*
245 *al.*, 2010) or *in vivo* (Niewold *et al.*, 1999). Despite lacking any sequence similarity, this group of
246 proteins shares a significant number of similar features, besides having the potential to form
247 amyloid-like fibrils.

248 A prominent example is *α*-crystallin, a small heat shock protein (sHSP), which is highly expressed
249 in the eye lens. Full-length *α*-crystallin has been found to form amyloid-like fibrils *in vitro*
250 (Ecroyd & Carver, 2009) and is believed to be implicated in the formation of cataract (Meehan *et*
251 *al*, 2004). As most sHSPs, *α*-crystallin exhibits remarkable structural plasticity, which is
252 intertwined with its chaperone activity (Basha *et al*, 2012). Interestingly, *α*-crystallin's
253 chaperone activity is exhibited in a very similar manner to that of clusterin (Carver *et al*, 2003).
254 sHSPs exist in solution as oligomeric structures, ranging from 9 to 50 subunits. Those structures
255 disassociate under stress and release functional subunits (Haslbeck & Buchner, 2002). *α*-
256 crystallin in particular, possesses a dynamic oligomeric structure, which, under increasing
257 temperature, allows exchange of subunits within proximate oligomers. The so-called "traveling
258 subunits" are believed to play a fundamental role in *α*-crystallin's chaperone activity, by
259 exposing hydrophobic surfaces and consequently, allowing hydrophobic interactions with
260 misfolded proteins, including A*β* (Doss *et al*, 1997; Inoue *et al*, 2016; Narayan *et al*, 2012). Even

261 though this is the physiological mechanism in which *α*-crystallin functions, it is reminiscent of
262 how amyloidogenic proteins behave on their way to self-assembly and formation of amyloid
263 fibrils (Cheon *et al*, 2007). This might explain the reports of *α*-crystallin forming amyloid-like
264 fibrils *in vitro (Ecroyd & Carver, 2009)*.

265 Another relevant example is that of the caseins, a group of proteins that comprise the largest
266 part of the total protein content in milk (Kunz & Lonnerdal, 1990) and are usually found in
267 aggregates, known as casein micelles. The micelles are primarily composed of four major
268 proteins, namely α_{s1}-, α_{s2}-, *β*- and *κ*-casein (McMahon & Oommen, 2008). All four of them have
269 been classified as intrinsically disordered proteins, because of the considerable structural
270 flexibility that they exhibit (Redwan *et al*, 2015). In consistence with clusterin and *α*-crystallin,
271 the major casein proteins are believed to function as molecular chaperones (Morgan *et al*,
272 2005), while *κ*-casein forms amyloid fibrils *in vitro* (Ecroyd *et al.*, 2010) and α_{s2}-casein forms
273 amyloid fibrils *in vivo*, in corpora amylacea, in the bovine mammary gland (Benson *et al.*, 2020;
274 Niewold *et al.*, 1999). Yet, in physiological conditions, α_{s1}-casein interacts with α_{s2}-casein,
275 forming α_s-casein, effectively halting the formation of amyloid fibrils (Thorn *et al*, 2008).
276 Similarly, α_s-casein and *β*-casein inhibit *κ*-casein amyloid formation, by shielding monomeric *κ*-
277 casein hydrophobic surfaces with similar regions of their respective sequences (Thorn *et al*,
278 2005).

279 In summary, clusterin, *α*-crystallin, and the casein proteins share common features:

280 (1) They function as molecular chaperones, by exposing hydrophobic regions, interacting with and
281 stabilizing misfolded proteins on their way to aggregation.
282 (2) They show structural plasticity, either having molten globule-like or intrinsically disordered
283 regions on their sequence.
284 (3) They are found in solution as heterogeneous aggregates, oligomers or micelles, which
285 dissociate under conditions of stress.
286 (4) They all interact with one, or more amyloidogenic proteins.

287 (5) Parts of their sequence, or the full-length proteins, are known to form amyloid-like fibrils *in*
288 *vitro* or *in vivo*.

289 These similarities may underlie a common mechanism in which the cell prevents toxic amyloid
290 formation under different conditions of stress, by utilizing the intrinsic amyloidogenicity of
291 specific molecular chaperones. For clusterin, amyloidogenesis inhibition could be activated
292 under pH-induced stress and achieved through the interaction of its aggregation-prone regions
293 with amyloidogenic proteins, on their way to aggregation. Likewise, *α*-crystallin could act under
294 temperature-induced stress and the casein proteins may present a more specific system of
295 amyloid inhibition, present primarily at the mammary gland.

296 **A putative mechanism for clusterin-mediated inhibition of A*β* amyloidogenesis**

297 Clusterin *α*-chain peptide-analogues can inhibit A*β* amyloidogenesis *in vitro*, and the structural
298 flexibility that natively disordered regions introduce, may enable them to act semi-
299 independently of the protein. Having established that, we opted to propose a mechanism in
300 which clusterin could use its aggregation-prone regions to exert its molecular chaperone activity
301 on A*β*.

302 It is believed that A*β* amyloidogenesis is promoted by acidic pH (Su & Chang, 2001). As
303 previously mentioned, mildly acidic pH also allows the disassociation of clusterin's
304 heterogeneous aggregates, releasing chaperone-active subunits (Poon *et al.*, 2002). In its
305 disassociated form, clusterin is assumed to hydrophobically interact with its client-proteins
306 through amphipathic *α*-helices, which are surrounded by molten globule-like regions (Bailey *et*
307 *al.*, 2001). ^{12}NFHAMFQ^{18}, one of clusterin's aggregation-prone regions, is located on a putative
308 amphipathic *α*-helix. However, we have already proved that NFHAMFQ also has the propensity
309 to form *β*-strands (Tsiolaki *et al.*, 2017), hinting that the broader region has the intrinsic
310 conformational properties of a chameleon sequence. When in proximity with an A*β* fibril, the *α*-
311 helical ^{12}NFHAMFQ^{18} could unfold and then refold into a *β*-strand, allowing interaction with A*β*'s

312 *β*-stranded regions and temporarily halting fibril growth. This process could trigger the
313 exposition of clusterin's other aggregation-prone regions and allow it to attach itself at the edge
314 of the A*β* fibril, via *β*-strand hydrogen bonding. In this manner, it would not allow A*β* monomers
315 to elongate the fibril, effectively blocking further polymerization. At the same time, free
316 clusterin subunits could bind to A*β* monomers, forming complexes and stabilizing their
317 structure, until it passes the baton to other molecular chaperones, once again, halting fiber
318 growth and minimizing the possibility of toxic secondary nucleation (Beeg *et al*, 2016). The
319 suggested mechanism is visualized in Fig 7.

320 The putative mechanism that was just described, is also supported by the identification of a
321 pathological mutation on clusterin's gene, in AD patients. As previously mentioned, p.I360N
322 changes the aggregation-prone region ^{81}ILSVD^{85} to ^{81}NLSVD^{85} (Bettens *et al.*, 2015). Considering
323 that out of the peptides we examined, ILSVD is hinted to be one of the better A*β* fibril formation
324 inhibitors, this mutation could lead to a malfunction in the clusterin-mediated amyloidogenesis
325 inhibition system. Thus, the pathogenicity of the phenotype could be explained by clusterin's
326 inability to inhibit amyloid formation, due to the absence of its most aggregation-prone region,
327 that being ^{81}ILSVD^{85}, which would normally inhibit A*β* fibril formation.

328 The aforementioned mechanism can explain why clusterin is found co-localized with A*β* fibrillar
329 deposits (Calero *et al.*, 2005) and is consistent with reports of clusterin decelerating A*β* fibril
330 formation (Beeg *et al.*, 2016; de Retana *et al*, 2019). However, clusterin's occasional
331 contribution to the appearance of AD symptoms (DeMattos *et al.*, 2002; Oh *et al.*, 2019) needs
332 further elucidation. It is logical to assume that, when A*β* misfolded monomers are produced
333 faster than what clusterin's existing population can process, the resulting complexes would fail
334 to stabilize A*β*'s structure, essentially bringing remote misfolded monomers into proximity. This
335 could accelerate amyloid fibril formation (Fig 6 – 6), while clusterin would end up co-localized
336 with the fibrillar deposits. This hypothesis is supported by the findings of Yerbury *et al*., which

337 show that clusterin's enhancing effect on amyloid formation is caused by low clusterin:substrate
338 ratio (Yerbury *et al.*, 2007). A relevant example could be found in patients with familial
339 Alzheimer's disease (FAD), where A*β* is produced much faster than usual (Wu *et al*, 2012). In
340 fact, most pre-clinical studies on AD use FAD animals as models, because it is a guaranteed
341 method of acquiring early-onset AD test subjects (LaFerla & Green, 2012). This could also be the
342 case for Oh *et. al*, who showed that clusterin-null 5XFAD mice, show AD symptoms later than
343 their littermate counterparts (Oh *et al.*, 2019). In the end, molecular chaperone-mediated
344 amyloidogenesis inhibition, seems to be a double-edged sword for the cell, effective, but at the
345 same time, conditionally harmful. The inadvertent bias that pre-clinical studies introduce, using
346 test subjects with FAD, rather than sporadic AD, could make the inhibition system seem much
347 more flawed than it really is.

348 **Peptide-based amyloidogenesis inhibitors, derived from aggregation-prone protein regions**

349 We ultimately proposed that the cell can prevent amyloid formation by utilizing the intrinsic
350 amyloidogenicity of specific molecular chaperones, similar to how functional amyloids work. If
351 that statement proves to be true, harnessing the ability of molecular chaperones to halt amyloid
352 formation could be essential to tackling AD and other amyloidoses. The key to inhibiting
353 amyloid formation lies in the aggregation-prone regions of said proteins, thus synthesizing and
354 studying peptides from such regions could provide novel inhibitors of A*β* amyloidogenesis and
355 amyloid formation in general (Connelly *et al*, 2010).

356 It is worth mentioning that, the ability of molecular chaperones to inhibit amyloid formation
357 doesn't seem to be substrate-specific, meaning that one chaperone could act as an
358 amyloidogenesis inhibitor for a variety of different amyloidogenic proteins, even if they are not
359 known to interact *in vivo*. For example, though *α*-crystallin is known to interact with A*β*
360 (Narayan *et al.*, 2012), the casein proteins are not. Despite that, all of them can inhibit A*β*
361 amyloidogenesis *in vitro (Carrotta et al, 2012; Raman et al, 2005)*. Furthermore, this also seems
362 to be the case for aggregation-prone peptides that are not derived from regions of molecular

363 chaperones (Lu *et al.*, 2019). Mimicking the physiological system for amyloidogenesis
364 prevention and extending it to aggregation-prone peptide-analogues of non-chaperone-active
365 proteins could provide us with a much greater variety of potential inhibitors.

366 Despite the potential that specific peptides show as amyloidogenesis inhibitors, it is of vital
367 importance to ensure that they are non-toxic for the cell. It is noteworthy that, even though
368 some molecular chaperones have amyloidogenic properties, they seem to not have negative
369 effects on the survival of the cell. In a similar manner, functional amyloids are not harmful to
370 the organisms in which they appear. It is believed that controlling the expression of
371 amyloidogenic proteins, regulating fibril formation with co-localized proteins-molecules and the
372 fact that they are often found isolated inside membrane bound compartments, are some of the
373 reasons why functional amyloids are not toxic (Jackson & Hewitt, 2017). For the peptide-
374 inhibitors to be usable, these questions must be accurately answered, and the findings should
375 be incorporated in their implementation as potential drugs for amyloidoses, especially when it
376 comes to peptide concentration and the complementary substances that should be
377 administered.

378 Materials and Methods

379 Prediction of potential aggregation-prone and natively disordered regions in human clusterin

380 AMYLPRED (Frousios *et al.*, 2009), a consensus algorithm for the prediction of amyloid
381 propensity, was used for the identification of aggregation-prone regions in wild-type, mature
382 clusterin (Uniprot AC: P10909). The α-chain, which is our focus in the current study, has five
383 such regions. The first one (^{12}NFHAMFQ^{18}) has previously been studied by our lab and proved to
384 exhibit amyloidogenic properties *in vitro* (Tsiolaki *et al.*, 2017). This time, we opted to study the
385 remaining four, those being ^{31}MDIHF^{35}, ^{82}LSV^{84}, ^{155}YYLRVTT^{161} and ^{177}EVVVKLF^{183}. Natively
386 disordered regions were predicted using PONDR® VLTX (http://www.pondr.com).

387 Peptide synthesis

388 All peptide-analogues were synthesized and lyophilized by GeneCust© Europe, France. The
389 exact sequences for the peptide-analogues were NFHAMFQ, AMDIHF, ILSVD, NLSVD, YYLRVTT
390 and EVVVKLF. The regions that were used for the second and third peptide-analogues were
391 ^{30}AMDIHF^{35} and ^{81}ILSVD^{85}, which are extensions of the original predicted regions. NLSVD is a
392 mutant counterpart of ILSVD. The purity of all the synthesized peptides was higher than 98%,
393 with the N- and C-terminals being free.

394 Aβ_{42} was also synthesized and lyophilized by GeneCust© Europe, France. The exact sequence is
395 DAEFRHDSGYEVHHQKLVFFAEDVGSNKGAIIGLMVGGVVIA. The purity of the peptide was higher
396 than 95%, with the N- and C-terminals being free.

397 **Sample preparation**

398 **Disaggregation of pre-existing aggregates:** Each lyophilized peptide was dissolved in
399 1,1,1,3,3,3-Hexafluoro-2-propanol (HFIP; Sigma©) at a concentration of 1 mg/mL. All clusterin
400 peptides were mixed with equimolar amounts of Aβ_{42}. Individual peptide solutions and Aβ_{42}-
401 clusterin peptide solutions were left to dry overnight in a fume hood, at room temperature, until
402 thin peptide-containing films were created. The peptide-containing films were stored at -20 °C.

403 ***In vitro* fibril formation:** The peptide-containing films were left at room temperature for 30
404 minutes and dissolved in 0.1 M HEPES buffer (pH=7.4; Sigma©) or dH_2O (pH=5.57), at
405 concentrations ranging from 10 µM to 1 mM. The peptide solutions were incubated for 1 week
406 at 37 °C, unless stated otherwise.

407 **Transmission Electron Microscopy (TEM).**

408 A 3 µL droplet of 100 or 500 µM peptide solution was applied to glow-discharged 400-mesh
409 carbon-coated copper grids for 60 seconds. Directly afterwards, the grids were stained with a 3
410 µL droplet of 2% (w/v) aqueous uranyl acetate for another 60 seconds. Excess stain was blotted
411 away with filter paper and air-dried. The grids were examined with a Morgagni™ 268

412 transmission electron microscope, operated at 80 kV. Digital acquisitions were performed with
413 an 11 Mpixel side mounted Morada CCD camera (Soft Imaging System, Muenster, Germany).

414 **X-ray diffraction from oriented protein fibers.**

415 **Oriented fiber formation:** 1 mM peptide solutions were incubated for two weeks, to form
416 viscous solutions, which facilitate the formation of oriented fibers. A 10 µL droplet of each
417 peptide solution was placed between two quartz capillaries covered with wax, spaced
418 approximately 1.5 mm apart and mounted horizontally on a glass substrate, as collinearly as
419 possible. The droplet was allowed to dry for 3 days, until oriented fibers were formed.

420 **X-ray diffraction and analysis:** The oriented fibers were shot with X-rays and diffracted. The X-
421 ray diffraction pattern was collected using a SuperNova-Agilent Technologies X-ray generator,
422 equipped with a 135 mm ATLAS CCD detector and a 4-circle kappa goniometer, at the Institute
423 of Biology, Medicinal Chemistry and Biotechnology, National Hellenic Research Foundation
424 (CuKα high intensity X-ray micro-focus source, λ = 1.5418 Å), operated at 50 kV, 0.8 mA. The
425 specimen-to-film distance was set at 52mm and the exposure time was set to 200s. The X-ray
426 patterns were initially viewed using CrysAlisPro (CrysAlis^{PRO}, 2014) and afterwards measured
427 with iMosFLM (Battye *et al*, 2011).

428 **Attenuated total reflectance Fourier-transform infrared (ATR FT-IR) spectroscopy.**

429 A 10 µL droplet of 500 µM peptide solution was cast on a front-coated Au mirror and left to dry
430 slowly at room temperature, until a thin peptide-containing film was created. Infrared spectra
431 were obtained from these films at a resolution of 4 cm^{-1}, utilizing an IR microscope (IRScope II by
432 Bruker Optics) equipped with a Ge attenuated total reflectance (ATR) objective lens (20x) and
433 attached to a Fourier-transform infrared (FT-IR) spectrometer (Equinox 55, by Bruker Optics).
434 Ten 32-scan spectra were collected from each sample and averaged to improve the sound/noise
435 (S/N) ratio. Both are shown in the absorption mode after correction for the wavelength
436 dependence of the penetration depth (pd-λ). Absorption band maxima were determined from

437 the minima in the second derivative of the corresponding spectra. Derivatives were computed
438 analytically using routines of the Bruker OPUS/OS2 software, including smoothing over a ±13
439 cm^{-1} range around each data point, performed by the Savitzky–Golay (Savitzky & Golay, 1964)
440 algorithm. Data was visualized using OriginPro 7 (OriginLab Corporation, Northampton, MA,
441 USA).

442 **Congo Red Birefringence Assay.**

443 A 3 µL droplet of the 500 µM peptide solution was applied to glass slides and stained with a 10
444 mM Congo Red (Sigma©) solution in PBS (137 mM NaCl, 27 mM KCl, 100 mM Na_2HPO_4, 18 mM
445 KH_2PO_4, pH=7.4) or dH_2O for approximately 30 minutes. Then, they were washed several times
446 with 90% ethanol and were left to dry approximately for 10 minutes. The samples were
447 observed under bright field illumination and between crossed polars, using a Leica MZ7.5
448 polarizing stereomicroscope, equipped with a Sony *α*6000 camera.

449 **Thioflavin T (ThT) Kinetic Assay**

450 ThT fluorescence measurements were conducted at 37 °C, in black 96-well plates with flat, clear
451 bottoms, using a Tecan Spark microplate reader. The top of the plates was sealed with
452 microplate covers and the fluorescence readings were performed through the bottom. A 444
453 nm filter was used for excitation and a 484 nm filter for emission. HFIP peptide films were
454 dissolved in DMSO and diluted in HEPES for a final DMSO concentration of less than 5% v/v. The
455 reaction solutions contained freshly prepared 10 µM disaggregated peptide solutions (individual
456 Aβ_{42} or Aβ_{42}-clusterin peptide solutions) and 25 µM ThT (Sigma©) in dH_2O. ThT background
457 fluorescence was measured in the absence of peptide solutions. Each experiment was
458 conducted in triplicates. Measurement lasted for 50 hours and fluorescence readings were
459 collected every 15 minutes. ThT background fluorescence was subtracted from the peptide
460 fluorescence readings at each time point. Standard deviation was calculated, and the data was

461 normalized. 100 arbitrary units correspond to maximum individual Aβ_{42} fluorescence intensity.
462 Data was visualized using RStudio (package ggplot2).

463 **Molecular Dynamics Simulations**

464 **Structure acquisition and molecular docking.** Simulations were performed using an NMR
465 structure of pentameric Aβ_{42} (PDB ID: 2BEG) (Luhrs *et al.*, 2005), while a structure for EVVVKLF
466 was generated through the "Builder" tool in PyMOL (Delano, 2005). Aβ_{42}-EVVVKLF docking was
467 performed through the automated protein docking server ClusPro (Kozakov *et al.*, 2013;
468 Kozakov *et al.*, 2017; Porter *et al.*, 2017; Vajda *et al.*, 2017). The generated clusters were
469 evaluated with the balanced scoring scheme.

470 **Molecular dynamics simulations.** The derived complex was subjected to molecular dynamics
471 simulations via GROMACS v. 2018.1 (Kutzner *et al*, 2019). The simulations employed the
472 AMBER99SB-ILDN protein, nucleic AMBER94 force-field (Lindorff-Larsen *et al*, 2010). The
473 complex was placed in a 1.2 nm cubic box of 3-point model (TIP3P) water (Jorgensen, 1983) and
474 the system was ionized using NaCl molecules, mimicking neutral pH conditions. Each simulation
475 system was subjected to energy minimization, in a maximum of 2000 steps, using the steepest
476 descent algorithm, followed by two stages of equilibration simulations with position restraints
477 applied on protein coordinates. Specifically, a 100 ps simulation was performed in the canonical
478 (NVT) ensemble to equilibrate temperature at 310 K, using the Berendsen-thermostat
479 (Berendsen, 1984). Following the first equilibration, a 100 ps simulation was performed in the
480 isothermal-isobaric (NPT) ensemble to control pressure isotopically at 1.013 bar (1 atm), using
481 the Berendsen weak coupling algorithm (Berendsen, 1991) and the Berendsen-thermostat at
482 310 K. Finally, the MD simulation with position restraints removed was carried out for 600ns at
483 310K. One control run of individual Aβ_{42} was also performed. Periodic boundary conditions
484 were applied to all directions. The LINCS algorithm (Berk Hess, 1997) was applied to model
485 bond constraints, enabling the use of a 2 fs time-step. Short range non-bonded interactions
486 were modeled using a twin-range cutoff at 0.8 nm, while long-range electrostatic interactions

487 were modeled using the Particle Mesh Ewald (PME) method, with a Fourier grid spacing at 0.12
488 nm (Essmann, 1995).

489 **Analysis of simulation results.** Simulation results were analyzed using various GROMACS
490 utilities, and Visual Molecular Dynamics (VMD) v. 1.9.4 (Humphrey *et al*, 1996). Structural
491 stability was checked using the "rms" tool (Maiorov & Crippen, 1995). Secondary structure was
492 calculated using the "do_dssp" tool (Kabsch & Sander, 1983; Touw *et al.*, 2015). Hydrogen
493 bonds were calculated using the "hbond" tool (van der Spoel *et al*, 2006). Frames were
494 extracted every 100ps and used for the analysis. Pictures were collected with UCSF Chimera
495 (Pettersen *et al.*, 2004) or PyMOL (Delano, 2005).

496 Availability of published material and data

497 This study includes no data deposited in external repositories.

498 Acknowledgments

499 This research has been co-financed by the European Union and Greek national funds through
500 the Operational Program "Competitiveness, Entrepreneurship and Innovation", under the call
501 "RESEARCH – CREATE – INNOVATE" (project code: T1EDK-00353). We acknowledge support of
502 this work by the project "INSPIRED-The National Research Infrastructures on Integrated
503 Structural Biology, Drug Screening Efforts and Drug target functional characterization" (MIS
504 5002550) which is implemented under the Action "Reinforcement of the Research and
505 Innovation Infrastructure", funded by the Operational Program "Competitiveness,
506 Entrepreneurship and Innovation" (NSRF 2014-2020) and co-funded by Greece and the
507 European Union (European Regional Development Fund). The molecular dynamics simulations
508 were performed utilizing computational time granted from the Greek Research & Technology
509 Network (GRNET) at the National HPC facility – ARIS under project ID "PR007003-
510 AbetaDynamics". We also acknowledge Dr. George Baltatzis for kindly assisting us with handling
511 the Morgagni Microscope at the 1st Department of Pathology, Medical School, National and

512 Kapodistrian University of Athens. Finally, we acknowledge the support of Dr. Aimilia Sklirou,
513 who kindly assisted with handling the Tecan Spark microplate reader.

514 Author contributions

515 P.M.S. performed sample preparation, Congo Red birefringence and ThT kinetics assays,
516 acquired and processed TEM, X-ray diffraction and ATR FT-IR spectroscopy data, analyzed the
517 molecular dynamics simulations results, helped in conceiving the project and wrote the initial
518 draft of the manuscript. G.I.N. participated and assisted in all the experiments. P.L.T. co-
519 supervised and helped in conceiving the project. M.K.T. performed the molecular dynamics
520 simulations and participated in the analysis of the results. N.C.P. supervised the molecular
521 dynamics simulations. I.P.T. helped in conceiving the project and supervised the ThT kinetics
522 assay. V.A.I. supervised and helped in conceiving the project. All authors discussed the results
523 and edited or commented on the manuscript.

524 Conflict of interest

525 The authors declare no conflicts of interest.

526 References

527 Bailey RW, Dunker AK, Brown CJ, Garner EC, Griswold MD (2001) Clusterin, a binding protein
528 with a molten globule-like region. *Biochemistry* 40: 11828-11840

529 Basha E, O'Neill H, Vierling E (2012) Small heat shock proteins and alpha-crystallins: dynamic
530 proteins with flexible functions. *Trends in biochemical sciences* 37: 106-117

531 Battye TG, Kontogiannis L, Johnson O, Powell HR, Leslie AG (2011) iMOSFLM: a new graphical
532 interface for diffraction-image processing with MOSFLM. *Acta crystallographica Section D,*
533 *Biological crystallography* 67: 271-281

534 Beeg M, Stravalaci M, Romeo M, Carra AD, Cagnotto A, Rossi A, Diomede L, Salmona M, Gobbi
535 M (2016) Clusterin Binds to Abeta1-42 Oligomers with High Affinity and Interferes with Peptide

536 Aggregation by Inhibiting Primary and Secondary Nucleation. *The Journal of biological chemistry*
537 291: 6958-6966
538 Benson MD, Buxbaum JN, Eisenberg DS, Merlini G, Saraiva MJM, Sekijima Y, Sipe JD,
539 Westermark P (2020) Amyloid nomenclature 2020: update and recommendations by the
540 International Society of Amyloidosis (ISA) nomenclature committee. *Amyloid : the international*
541 *journal of experimental and clinical investigation : the official journal of the International Society*
542 *of Amyloidosis* 27: 217-222
543 Berendsen HJC (1991) Transport Properties Computed by Linear Response through Weak
544 Coupling to a Bath. In: *Computer Simulation in Materials Science*, pp. 139-155. Springer,
545 Dordrecht:
546 Berendsen HJC, Postma, J. P. M., Van Gunsteren, W. F., Dinola, A., & Haak, J. R. (1984) Molecular
547 dynamics with coupling to an external bath. *The Journal of Chemical Physics* 81
548 Berk Hess HB, Herman J. C. Berendsen, Johannes G. E. M. Fraaije (1997) LINCS: A linear
549 constraint solver for molecular simulations. *Journal of Computational Chemistry* 18: 1463-1472
550 Bettens K, Vermeulen S, Van Cauwenberghe C, Heeman B, Asselbergh B, Robberecht C,
551 Engelborghs S, Vandenbulcke M, Vandenberghe R, De Deyn PP *et al* (2015) Reduced secreted
552 clusterin as a mechanism for Alzheimer-associated CLU mutations. *Molecular*
553 *neurodegeneration* 10: 30
554 Calero M, Rostagno A, Frangione B, Ghiso J (2005) Clusterin and Alzheimer's disease. *Sub-cellular*
555 *biochemistry* 38: 273-298
556 Carrotta R, Canale C, Diaspro A, Trapani A, Biagio PL, Bulone D (2012) Inhibiting effect of
557 alpha(s1)-casein on Abeta(1-40) fibrillogenesis. *Biochimica et biophysica acta* 1820: 124-132
558 Carver JA, Rekas A, Thorn DC, Wilson MR (2003) Small heat-shock proteins and clusterin: intra-
559 and extracellular molecular chaperones with a common mechanism of action and function?
560 *IUBMB life* 55: 661-668

561 Chafekar SM, Malda H, Merkx M, Meijer EW, Viertl D, Lashuel HA, Baas F, Scheper W (2007)
562 Branched KLVFF tetramers strongly potentiate inhibition of beta-amyloid aggregation.
563 *Chembiochem* 8: 1857-1864
564 Cheon M, Chang I, Mohanty S, Luheshi LM, Dobson CM, Vendruscolo M, Favrin G (2007)
565 Structural reorganisation and potential toxicity of oligomeric species formed during the
566 assembly of amyloid fibrils. *PLoS computational biology* 3: 1727-1738
567 Connelly S, Choi S, Johnson SM, Kelly JW, Wilson IA (2010) Structure-based design of kinetic
568 stabilizers that ameliorate the transthyretin amyloidoses. *Current opinion in structural biology*
569 20: 54-62
570 CrysAlis^{PRO}, 2014. Agilent Technologies, Version 1.171.37.31 ed. Agilent Technologies UK Ltd,
571 Oxford, UK, p. Software system.
572 de Retana SF, Marazuela P, Sole M, Colell G, Bonaterra A, Sanchez-Quesada JL, Montaner J,
573 Maspoch D, Cano-Sarabia M, Hernandez-Guillamon M (2019) Peripheral administration of
574 human recombinant ApoJ/clusterin modulates brain beta-amyloid levels in APP23 mice.
575 *Alzheimer's research & therapy* 11: 42
576 Delano WL, 2005. The PyMOL Molecular Graphics System. DeLano Scientific LLC
577 400, Oyster Point Blvd., Suite 213, South San Francisco, CA 94080-1918, USA.
578 DeMattos RB, O'Dell M A, Parsadanian M, Taylor JW, Harmony JA, Bales KR, Paul SM, Aronow BJ,
579 Holtzman DM (2002) Clusterin promotes amyloid plaque formation and is critical for neuritic
580 toxicity in a mouse model of Alzheimer's disease. *Proceedings of the National Academy of*
581 *Sciences of the United States of America* 99: 10843-10848
582 Doss EW, Ward KA, Koretz JF (1997) Preliminary studies on the aggregation process of alpha-
583 crystallin. *Experimental eye research* 65: 255-266
584 Ecroyd H, Carver JA (2009) Crystallin proteins and amyloid fibrils. *Cellular and molecular life*
585 *sciences : CMLS* 66: 62-81

586 Ecroyd H, Thorn DC, Liu Y, Carver JA (2010) The dissociated form of kappa-casein is the
587 precursor to its amyloid fibril formation. *The Biochemical journal* 429: 251-260
588 Essmann U, Perera, L., Berkowitz, M. L., Darden, T., Lee, H., & Pedersen, L. G. (1995) A smooth
589 particle mesh Ewald method. *The Journal of Chemical Physics* 103
590 Frousios KK, Iconomidou VA, Karletidi CM, Hamodrakas SJ (2009) Amyloidogenic determinants
591 are usually not buried. *BMC structural biology* 9: 44
592 Haslbeck M, Buchner J (2002) Chaperone function of sHsps. *Progress in molecular and*
593 *subcellular biology* 28: 37-59
594 Humphrey W, Dalke A, Schulten K (1996) VMD: visual molecular dynamics. *J Mol Graph* 14: 33-
595 38, 27-38
596 Inoue R, Takata T, Fujii N, Ishii K, Uchiyama S, Sato N, Oba Y, Wood K, Kato K, Fujii N *et al* (2016)
597 New insight into the dynamical system of alphaB-crystallin oligomers. *Scientific reports* 6: 29208
598 Jackson MP, Hewitt EW (2017) Why are Functional Amyloids Non-Toxic in Humans?
599 *Biomolecules* 7
600 Jones SE, Jomary C (2002) Clusterin. *The international journal of biochemistry & cell biology* 34:
601 427-431
602 Jorgensen WL, Chandrasekhar, J., Madura, J. D., Impey, R. W., & Klein, M. L. (1983) Comparison
603 of simple potential functions for simulating liquid water. *The Journal of Chemical Physics* 79
604 Kabsch W, Sander C (1983) Dictionary of protein secondary structure: pattern recognition of
605 hydrogen-bonded and geometrical features. *Biopolymers* 22: 2577-2637
606 Kozakov D, Beglov D, Bohnuud T, Mottarella SE, Xia B, Hall DR, Vajda S (2013) How good is
607 automated protein docking? *Proteins* 81: 2159-2166
608 Kozakov D, Hall DR, Xia B, Porter KA, Padhorny D, Yueh C, Beglov D, Vajda S (2017) The ClusPro
609 web server for protein-protein docking. *Nat Protoc* 12: 255-278

610 Kunz C, Lonnerdal B (1990) Human-milk proteins: analysis of casein and casein subunits by
611 anion-exchange chromatography, gel electrophoresis, and specific staining methods. *The*
612 *American journal of clinical nutrition* 51: 37-46
613 Kutzner C, Pall S, Fechner M, Esztermann A, de Groot BL, Grubmuller H (2019) More bang for
614 your buck: Improved use of GPU nodes for GROMACS 2018. *J Comput Chem* 40: 2418-2431
615 Kyle RA (2011) Amyloidosis: a brief history. *Amyloid : the international journal of experimental*
616 *and clinical investigation : the official journal of the International Society of Amyloidosis* 18 Suppl
617 1: 6-7
618 LaFerla FM, Green KN (2012) Animal models of Alzheimer disease. *Cold Spring Harbor*
619 *perspectives in medicine* 2
620 Lindorff-Larsen K, Piana S, Palmo K, Maragakis P, Klepeis JL, Dror RO, Shaw DE (2010) Improved
621 side-chain torsion potentials for the Amber ff99SB protein force field. *Proteins* 78: 1950-1958
622 Lu J, Cao Q, Wang C, Zheng J, Luo F, Xie J, Li Y, Ma X, He L, Eisenberg D *et al* (2019) Structure-
623 Based Peptide Inhibitor Design of Amyloid-beta Aggregation. *Frontiers in molecular neuroscience*
624 12: 54
625 Luhrs T, Ritter C, Adrian M, Riek-Loher D, Bohrmann B, Dobeli H, Schubert D, Riek R (2005) 3D
626 structure of Alzheimer's amyloid-beta(1-42) fibrils. *Proceedings of the National Academy of*
627 *Sciences of the United States of America* 102: 17342-17347
628 Maiorov VN, Crippen GM (1995) Size-independent comparison of protein three-dimensional
629 structures. *Proteins: Structure, Function, and Genetics* 22: 273-283
630 Makin OS, Serpell LC (2005) X-ray diffraction studies of amyloid structure. *Methods in molecular*
631 *biology* 299: 67-80
632 Matsubara E, Soto C, Governale S, Frangione B, Ghiso J (1996) Apolipoprotein J and Alzheimer's
633 amyloid beta solubility. *The Biochemical journal* 316 (Pt 2): 671-679
634 McMahon DJ, Oommen BS (2008) Supramolecular structure of the casein micelle. *Journal of*
635 *dairy science* 91: 1709-1721

636 Meehan S, Berry Y, Luisi B, Dobson CM, Carver JA, MacPhee CE (2004) Amyloid fibril formation
637 by lens crystallin proteins and its implications for cataract formation. *The Journal of biological*
638 *chemistry* 279: 3413-3419
639 Morgan PE, Treweek TM, Lindner RA, Price WE, Carver JA (2005) Casein proteins as molecular
640 chaperones. *Journal of agricultural and food chemistry* 53: 2670-2683
641 Narayan P, Meehan S, Carver JA, Wilson MR, Dobson CM, Klenerman D (2012) Amyloid-beta
642 oligomers are sequestered by both intracellular and extracellular chaperones. *Biochemistry* 51:
643 9270-9276
644 Nastou KC, Nasi GI, Tsiolaki PL, Litou ZI, Iconomidou VA (2019) AmyCo: the amyloidoses
645 collection. *Amyloid : the international journal of experimental and clinical investigation : the*
646 *official journal of the International Society of Amyloidosis* 26: 112-117
647 Niewold TA, Murphy CL, Hulskamp-Koch CA, Tooten PC, Gruys E (1999) Casein related amyloid,
648 characterization of a new and unique amyloid protein isolated from bovine corpora amylacea.
649 *Amyloid : the international journal of experimental and clinical investigation : the official journal*
650 *of the International Society of Amyloidosis* 6: 244-249
651 Oh SB, Kim MS, Park S, Son H, Kim SY, Kim MS, Jo DG, Tak E, Lee JY (2019) Clusterin contributes
652 to early stage of Alzheimer's disease pathogenesis. *Brain pathology* 29: 217-231
653 Pettersen EF, Goddard TD, Huang CC, Couch GS, Greenblatt DM, Meng EC, Ferrin TE (2004) UCSF
654 Chimera?A visualization system for exploratory research and analysis. *Journal of Computational*
655 *Chemistry* 25: 1605-1612
656 Poon S, Easterbrook-Smith SB, Rybchyn MS, Carver JA, Wilson MR (2000) Clusterin is an ATP-
657 independent chaperone with very broad substrate specificity that stabilizes stressed proteins in
658 a folding-competent state. *Biochemistry* 39: 15953-15960
659 Poon S, Rybchyn MS, Easterbrook-Smith SB, Carver JA, Pankhurst GJ, Wilson MR (2002) Mildly
660 acidic pH activates the extracellular molecular chaperone clusterin. *The Journal of biological*
661 *chemistry* 277: 39532-39540

662 Porter KA, Xia B, Beglov D, Bohnuud T, Alam N, Schueler-Furman O, Kozakov D (2017) ClusPro
663 PeptiDock: efficient global docking of peptide recognition motifs using FFT. *Bioinformatics* 33:
664 3299-3301
665 Raman B, Ban T, Sakai M, Pasta SY, Ramakrishna T, Naiki H, Goto Y, Rao Ch M (2005) AlphaB-
666 crystallin, a small heat-shock protein, prevents the amyloid fibril growth of an amyloid beta-
667 peptide and beta2-microglobulin. *The Biochemical journal* 392: 573-581
668 Redwan EM, Xue B, Almehdar HA, Uversky VN (2015) Disorder in milk proteins: caseins,
669 intrinsically disordered colloids. *Current protein & peptide science* 16: 228-242
670 Rohne P, Prochnow H, Koch-Brandt C (2016) The CLU-files: disentanglement of a mystery.
671 *Biomolecular concepts* 7: 1-15
672 Savitzky A, Golay MJE (1964) Smoothing and Differentiation of Data by Simplified Least Squares
673 Procedures. *Analytical Chemistry* 36: 1627-1639
674 Su Y, Chang PT (2001) Acidic pH promotes the formation of toxic fibrils from beta-amyloid
675 peptide. *Brain research* 893: 287-291
676 Sunde M, Blake CC (1998) From the globular to the fibrous state: protein structure and
677 structural conversion in amyloid formation. *Quarterly reviews of biophysics* 31: 1-39
678 Surewicz WK, Mantsch HH, Chapman D (1993) Determination of protein secondary structure by
679 Fourier transform infrared spectroscopy: a critical assessment. *Biochemistry* 32: 389-394
680 Teng PK, Eisenberg D (2009) Short protein segments can drive a non-fibrillizing protein into the
681 amyloid state. *Protein engineering, design & selection : PEDS* 22: 531-536
682 Thorn DC, Ecroyd H, Sunde M, Poon S, Carver JA (2008) Amyloid fibril formation by bovine milk
683 alpha s2-casein occurs under physiological conditions yet is prevented by its natural
684 counterpart, alpha s1-casein. *Biochemistry* 47: 3926-3936
685 Thorn DC, Meehan S, Sunde M, Rekas A, Gras SL, MacPhee CE, Dobson CM, Wilson MR, Carver
686 JA (2005) Amyloid fibril formation by bovine milk kappa-casein and its inhibition by the
687 molecular chaperones alphaS- and beta-casein. *Biochemistry* 44: 17027-17036

688 Touw WG, Baakman C, Black J, te Beek TAH, Krieger E, Joosten RP, Vriend G (2015) A series of
689 PDB-related databanks for everyday needs. *Nucleic Acids Research* 43: D364-D368
690 Tsiolaki PL, Nastou KC, Louros NN, Hamodrakas SJ, Iconomidou VA (2017) Exploring
691 Amyloidogenicity of Clusterin: A Structural and Bioinformatics Analysis. *Advances in*
692 *experimental medicine and biology* 989: 93-107
693 Vajda S, Yueh C, Beglov D, Bohnuud T, Mottarella SE, Xia B, Hall DR, Kozakov D (2017) New
694 additions to the ClusPro server motivated by CAPRI. *Proteins* 85: 435-444
695 van der Spoel D, van Maaren PJ, Larsson P, Tîmneanu N (2006) Thermodynamics of Hydrogen
696 Bonding in Hydrophilic and Hydrophobic Media. *The Journal of Physical Chemistry B* 110: 4393-
697 4398
698 Wentink A, Nussbaum-Krammer C, Bukau B (2019) Modulation of Amyloid States by Molecular
699 Chaperones. *Cold Spring Harbor perspectives in biology*
700 Wu L, Rosa-Neto P, Hsiung GY, Sadovnick AD, Masellis M, Black SE, Jia J, Gauthier S (2012) Early-
701 onset familial Alzheimer's disease (EOFAD). *The Canadian journal of neurological sciences Le*
702 *journal canadien des sciences neurologiques* 39: 436-445
703 Yerbury JJ, Kumita JR (2010) Protein chemistry of amyloid fibrils and chaperones: implications
704 for amyloid formation and disease. *Current Chemical Biology* 4: 89-98
705 Yerbury JJ, Poon S, Meehan S, Thompson B, Kumita JR, Dobson CM, Wilson MR (2007) The
706 extracellular chaperone clusterin influences amyloid formation and toxicity by interacting with
707 prefibrillar structures. *FASEB journal : official publication of the Federation of American Societies*
708 *for Experimental Biology* 21: 2312-2322

709

710 **Figure legends**

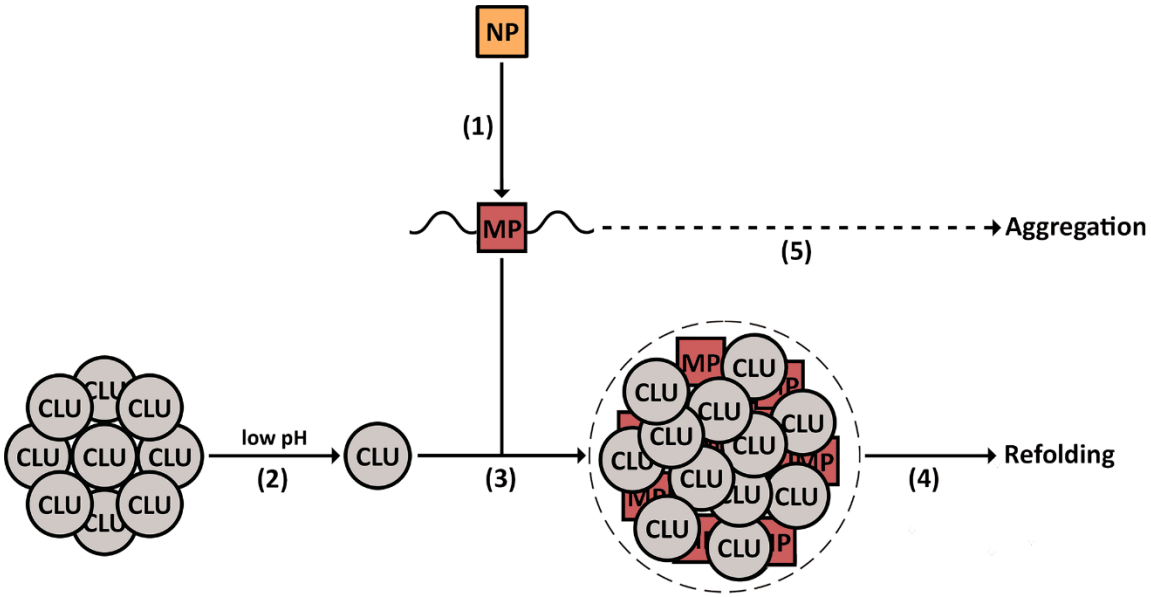

711

712 Figure 1. Representation of clusterin's molecular chaperone activity. (1) Under stress (low pH), native proteins (NP)
713 may partially unfold and become misfolded. (2) At slightly acidic pH, clusterin's (CLU) oligomers start disassociating
714 and the chaperone-active clusterin subunits get released. (3) The free clusterin subunits bind the misfolded proteins
715 (MP) and form a complex, effectively stabilizing them, (4) while other molecular chaperones refold them to their
716 native state. (5) If this mechanism proves ineffective, the misfolded proteins may form aggregates.

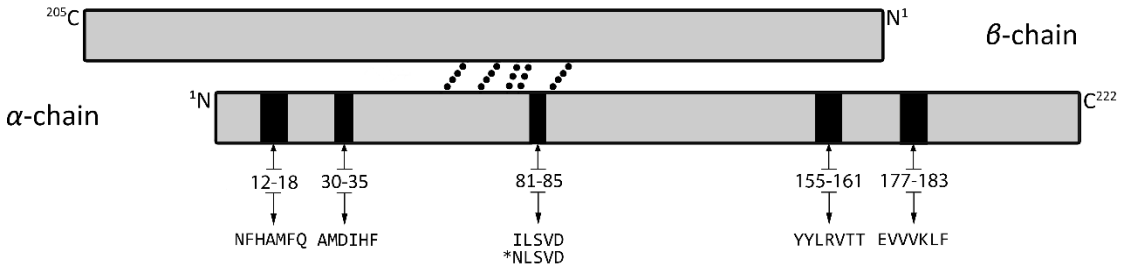

Figure 2. A simple representation of clusterin's two chains. Each chain is colored grey, with a black outline, and its sequence is numbered as found in the mature protein. The *α*-chain consists of 222 amino acid residues. The *β*-chain is slightly shorter, consisting of 205 amino acid residues. The two chains are joined by five disulfide bonds, depicted as black dots. The aggregation-prone regions of the *α*-chain are depicted as black rectangles on clusterin's sequence.

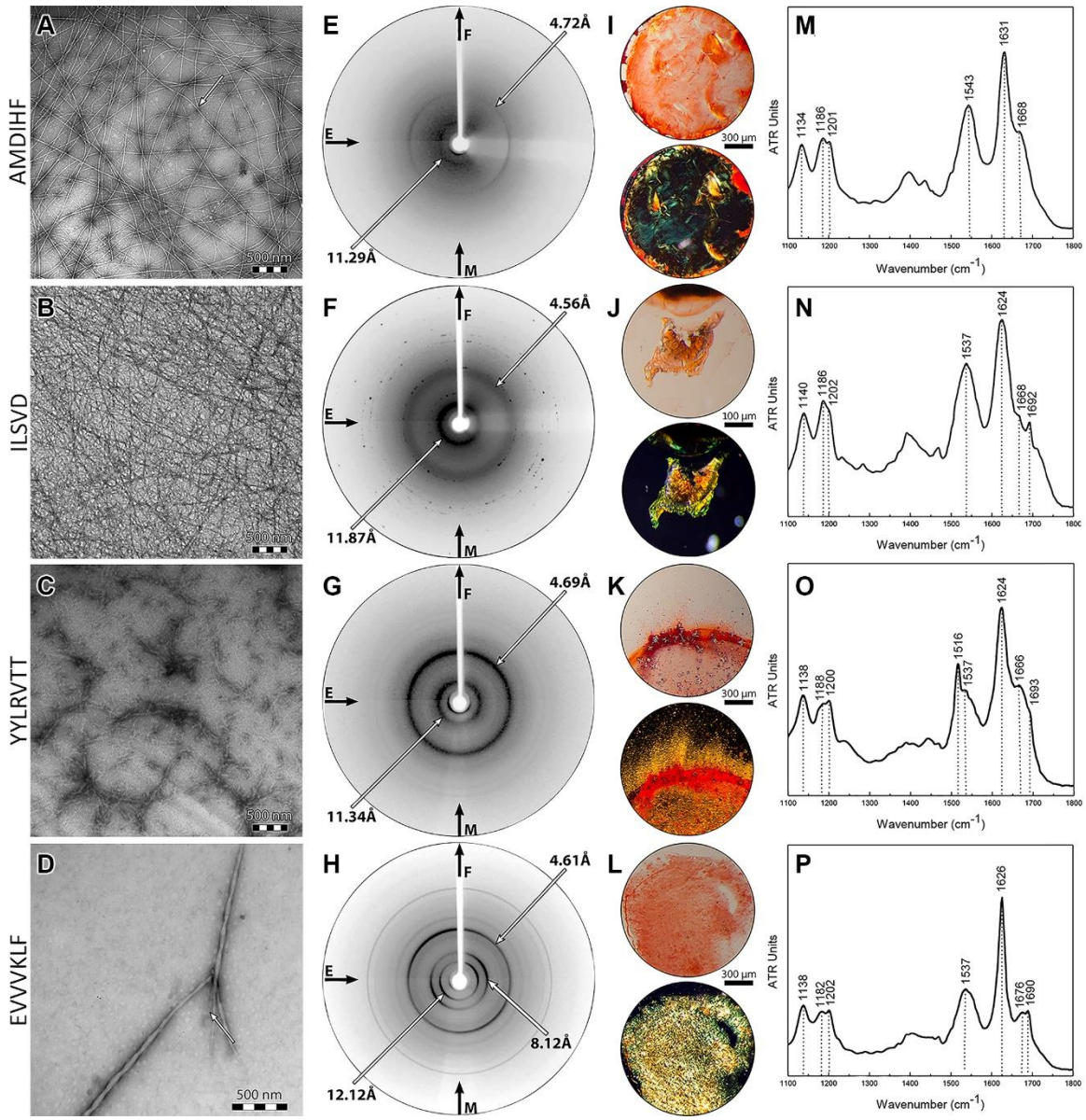

Figure 3. All the peptide-analogues fulfill the experimental criteria. (A-D) Transmission electron micrographs of amyloid-like fibrils derived from 500 µm solutions of peptides AMDIHF, ILSVD, YYLRVTT and EVVVKLF, respectively. White arrows mark single fibrils with the diameter of typical amyloid fibrils. (E-H) X-ray diffraction patterns of oriented fibers, derived from 1 mM solutions of the four peptides, respectively. Reflections marked with arrows are indicative of the "cross-*β*" structure, which amyloids typically have. (I-L) Photomicrographs of gels, derived from 500 µM solutions of the four peptides, respectively. Congo red is bound, as seen under bright field illumination (upper). The apple-green birefringence that amyloids typically exhibit is observed under crossed polars (lower). (M-P) ATR FT-IR spectra (1100–1800 cm^{-1}) produced from thin hydrated films created by 500 µM solutions of the four peptides, respectively. Fibrils derived from each peptide has *β*-sheet secondary structure, as hinted by the presence of strong amide I and II bands.

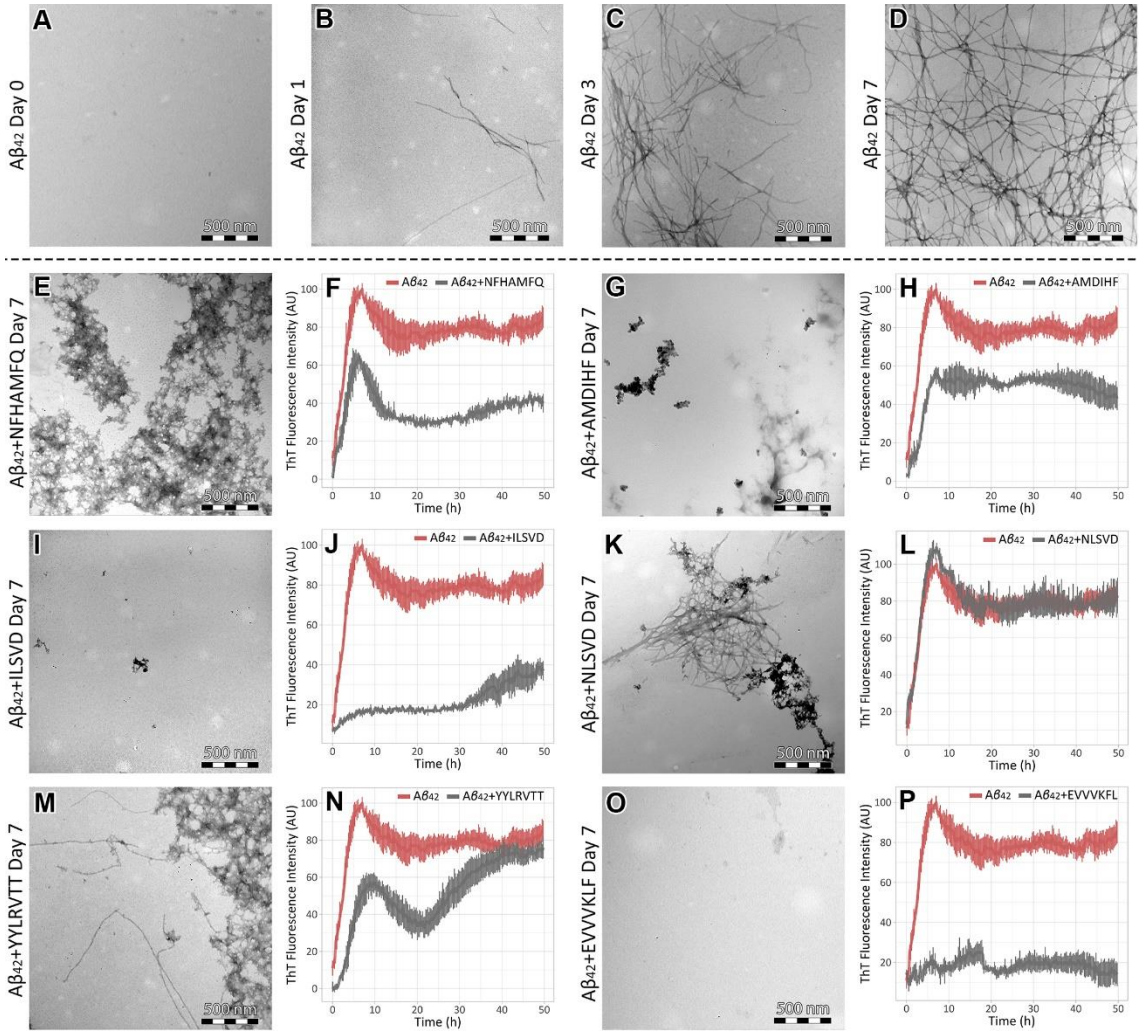

Figure 4. Clusterin peptide-analogues inhibit or delay Aβ_{42} fibril formation. (A-D) Transmission electron micrographs of Aβ_{42}, incubated for 0, 1, 3 and 7 days, respectively. Amyloid fibrils are observed from day 1 to day 7. The number of fibrils raises as incubation time increases. (E, F) Transmission electron micrograph and ThT fluorescence emission spectrum of Aβ_{42} co-incubated with NFHAMFQ for 7 days and over a period of 50 hours, respectively. (G, H) Transmission electron micrograph and ThT fluorescence emission spectrum of Aβ_{42} co-incubated with AMDIHF for 7 days and over a period of 50 hours, respectively. (I, J) Transmission electron micrograph and ThT fluorescence emission spectrum of Aβ_{42} co-incubated with ILSVD for 7 days and over a period of 50 hours, respectively. (K, L) Transmission electron micrograph and ThT fluorescence emission spectrum of Aβ_{42} co-incubated with the mutant peptide, NLSVD, for 7 days and over a period of 50 hours, respectively. (M, N) Transmission electron micrograph and ThT fluorescence emission spectrum of Aβ_{42} co-incubated with YYLRVTT for 7 days and over a period of 50 hours, respectively. (O, P) Transmission electron micrograph and ThT fluorescence emission spectrum of Aβ_{42} co-incubated with EVVVKLF for 7 days and over a period of 50 hours, respectively. Error bars in ThT fluorescence emission spectra represent standard deviation among triplicates. TEM experiments contained 100 µM Aβ_{42} and 100 µM clusterin peptide-analogues, while ThT experiments contained 10 µM and 10 µM, respectively.

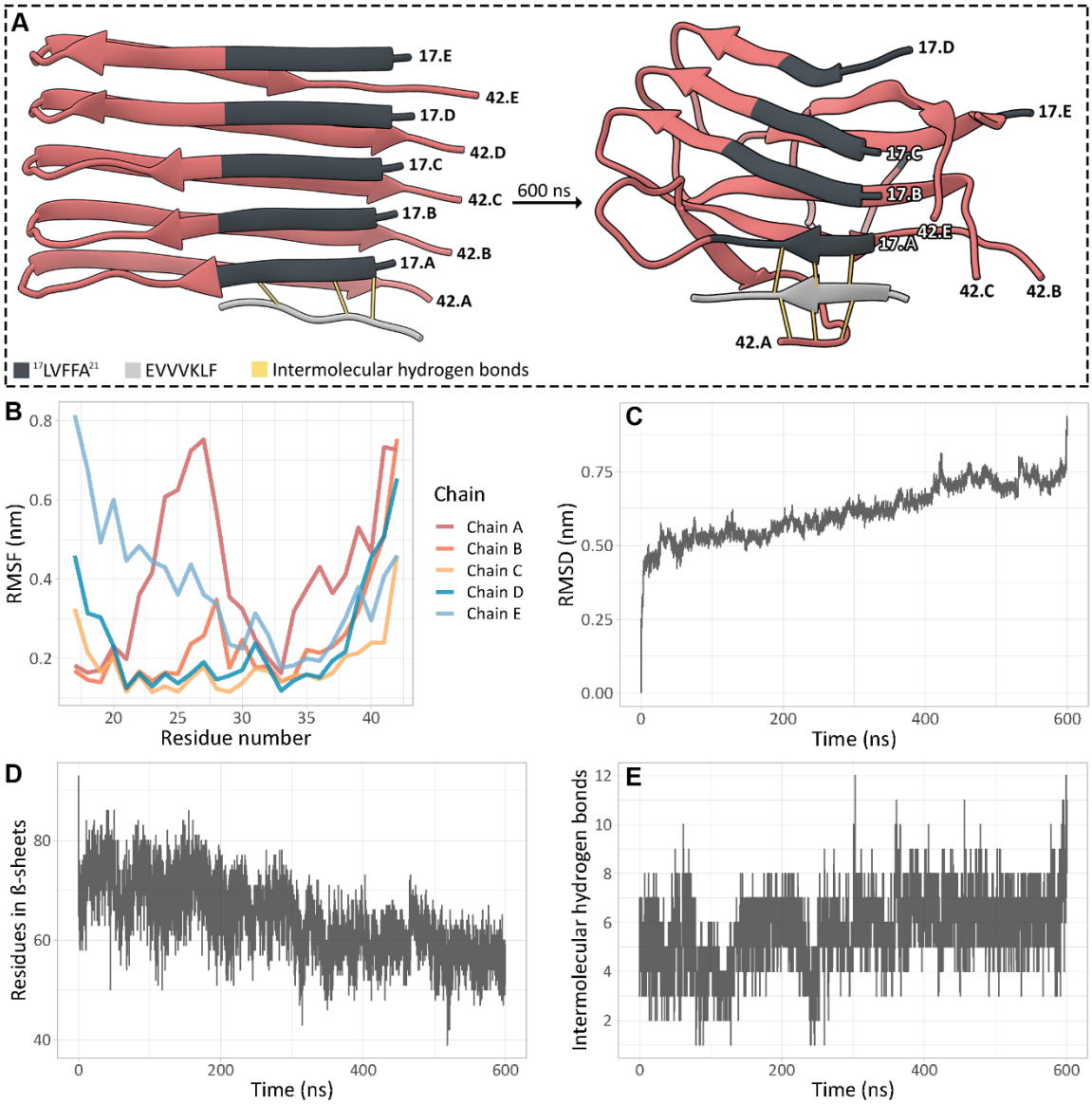

Figure 5. Results of molecular dynamics simulations for Aβ_{42}+EVVVKLF. (A) First (0 ns, left) and last (600 ns, right) frames of the molecular dynamics simulation. The position of the N- and C-terminals of each Aβ_{42} chain are marked on each frame (17.A-17.E and 42.A-42.E, respectively). EVVVKLF (light grey) forms hydrogen bonds (yellow lines) with the chain-A ^{17}LVFFA^{21} (dark grey), right after molecular docking and energy minimization. More bonds are formed by the end of the simulation. (B) RMSF per residue plot, after 600 ns of molecular dynamics simulations. (C) RMSD over time plot. (D) Total number of residues in β-sheets, according to DSSP, over time. (E) Number of intermolecular hydrogens bonds, between Aβ_{42} and EVVVKLF, over time.

```
                        Amphipathic α-helix
1       SLMPFSPYEP LNFHAMFQPF LEMIHEAQQA MDIHFHSPAF QHPPTEFIRE
PONDR   DDDDDD

51      GDDDRTVCRE IRHNSTGCLR MKDQCDKCRE ILSVDCSTNN PSQAKLRREL
PONDR                  DDDDDD D                    D DDDDDDDDDD
            Amphipathic α-helix
101     DESLQVAERL TRKYNELLKS YQWKMLNTSS LLEQLNEQFN WVSRLANLTQ
PONDR   DDDDDDDDDD

151     GEDQYYLRVT TVASHTSDSD VPSGVTEVVV KLFDSDPITV TVPVEVSRKN
PONDR                DDDDDDDD DDDDDDDDDD D            DDDDDDDDD
          Amphipathic α-helix
201     PKFMETVAEK ALQEYRKKHR EE
PONDR   DDDDDDDDDD DDDDDDDDDD DD
```

Figure 6. Relative position of natively disordered regions (as predicted by PONDR® VLTX), aggregation-prone regions, and putative amphipathic α-helices, on the sequence of human clusterin α-chain. All aggregation-prone regions are located near predicted natively disordered regions. ^{12}NFHAMFQ^{18} is located on a putative amphipathic α-helix, while ^{177}EVVVKLF^{183} is partly predicted as natively disordered.

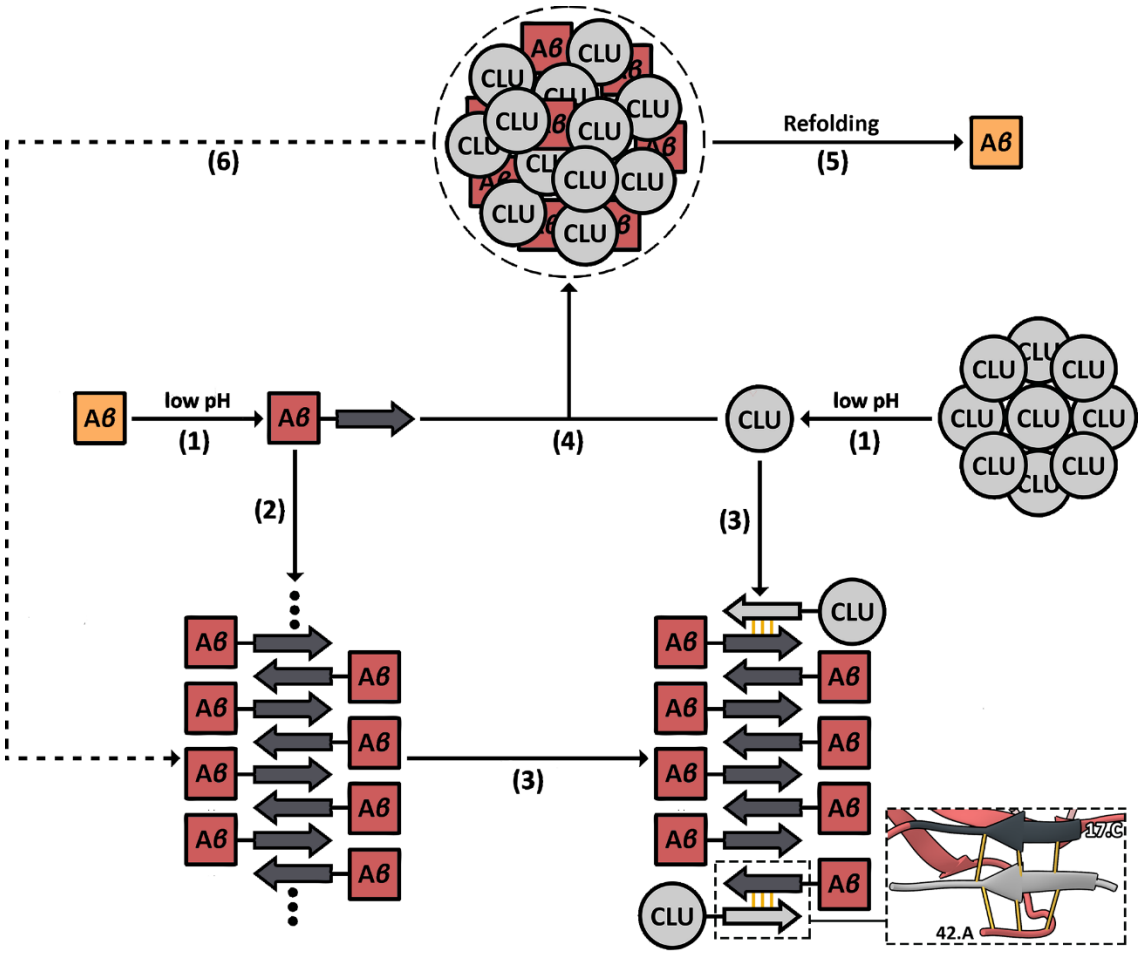

Figure 7. Putative mechanism of clusterin-mediated inhibition of Aβ amyloidogenesis. (1) Under acidic pH-induced stress, Aβ may partially unfold, exposing hydrophobic regions with the propensity to form β-strands. At the same time, the acidic pH triggers the disassociation of clusterin's heterogeneous aggregates. (2) Misfolded Aβ begin to form amyloid fibrils, but (3) the disassociated clusterin subunits (CLU) halt fibril growth, utilizing their aggregation-prone regions, which tend to form β-strands as well. The outlined picture is derived from the last frame of the molecular dynamics simulation of $A\beta_{42}$+EVVVKLF. (4) Clusterin binds misfolded Aβ monomers, forming complexes and stabilizes their structure, until (5) they are refolded by other molecular chaperones. (6) In case misfolded Aβ species are produced faster than clusterin can stabilize their structure, it essentially brings them into proximity with remote monomers, accelerating amyloid formation.

771 Table 1. Bands observed in the ATR FT-IR spectra obtained from thin hydrated films produced by AMDIHF, EVVVKLF,
772 YYLRVTT and ILSVD solutions, respectively, and their tentative assignments.

AMDIHF bands	ILSVD bands	YYLRVTT bands	EVVVKLF bands	Band assignments
1134	1140	1138	1138	TFA
1186	1186	1188	1182	TFA
1201	1202	1200	1202	TFA
-	-	1516	-	Tyrosine
1543	1537	1537	1537	*β*-sheet
1631	1624	1624	1626	*β*-sheet
1668	1668	1666	1676	TFA
-	1692	1693	1690	Antiparallel *β*-sheet

773

774 **Expanded View**

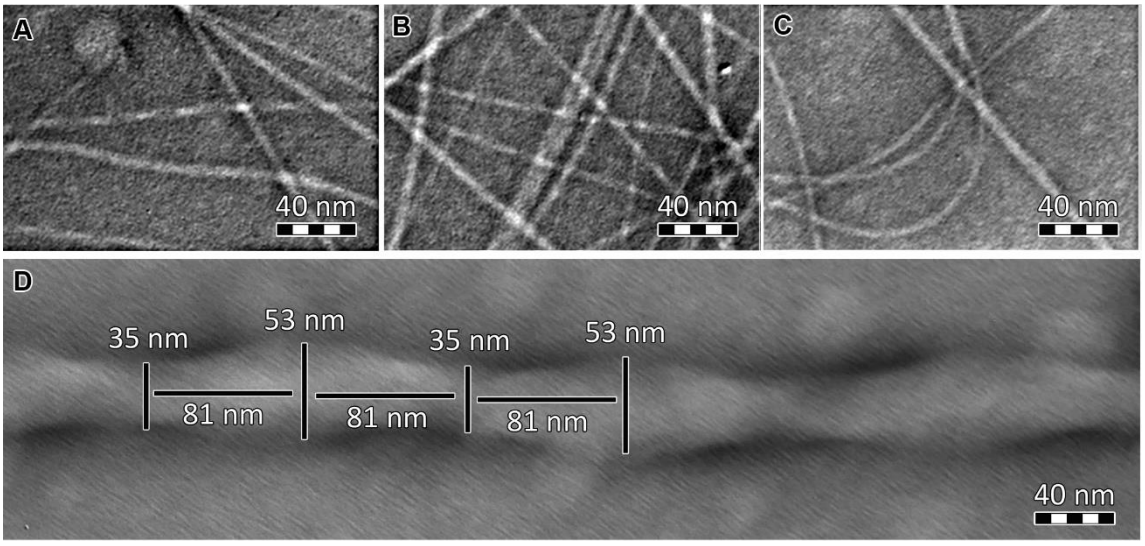

775

776 Figure EV1. Electron micrographs of polymorphic structures formed by AMDIHF and EVVVKLF amyloid-like fibrils,
777 after 7 days of incubation, at 500 µM. (A) Supercoil formed by AMDIHF amyloid-like fibrils. (B) Tape formed by
778 laterally interacting AMDIHF amyloid-like fibrils. (C) An amyloid-like fibril formed by AMDIHF, with a diameter of
779 approximately 160 Å, is split into two 80 Å fibrils. (D) EVVVKLF amyloid-like fibrils form large, twisting ribbons, with a
780 162 nm pitch, a minimum width of 35 nm, and a maximum width of 53 nm.

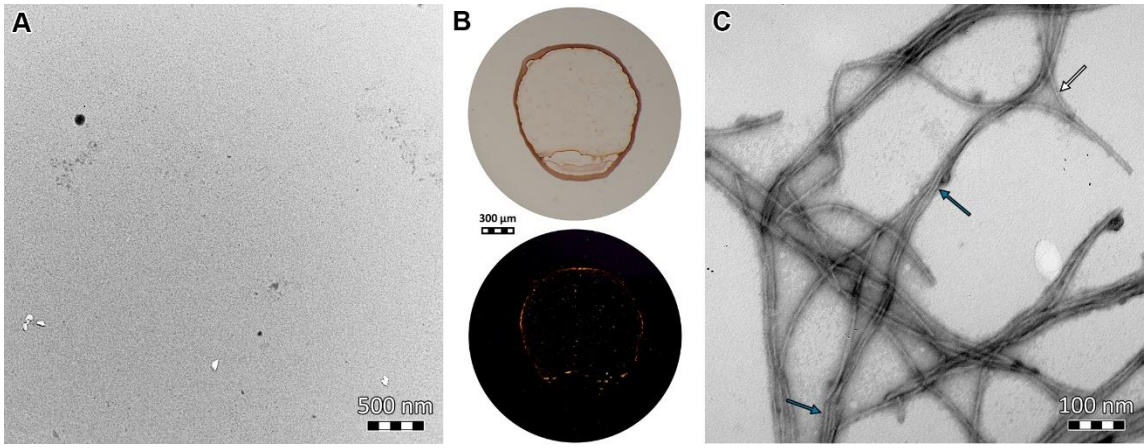

Figure EV2. The mutant NLSVD does not form amyloid-like fibrils and does not inhibit Aβ_{42} fibril formation. (A) Electron micrographs reveal that NLSVD 500 µM solution does not contain amyloid-like fibrils, after 7 days of incubation. (B) Photomicrographs of gels derived from NLSVD 500 µM solution. Congo red is faintly bound, as seen under bright field illumination (upper) and apple-green birefringence is not exhibited under crossed polars (lower). (C) Electron micrographs of Aβ_{42}+NLSVD (100 µM Aβ_{42} and 100 µM NLSVD) reveal that NLSVD does not inhibit amyloid fibril formation, after 7 days of incubation. Aβ_{42} fibrils (white arrow) are wider than those of individually incubated Aβ_{42} fibrils (Figure 4d) and have a higher tendency to interact laterally and form loosely bound tapes (blue arrows).